Title

Iron Speciation in PM2.5 From Urban, Agriculture, and Mixed Environments in Colorado, USA

Journal

Earth and Space Science, 7(10)

ISSN

2333-5084

Authors

Salazar, Joseph R

Pfotenhauer, David J

Leresche, Frank

et al.

Publication Date

2020-10-01

DOI

10.1029/2020ea001262

Peer reviewed

AGU ADVANCING EARTH AND SPACE SCIENCE

Earth and Space Science

RESEARCH ARTICLE
10.1029/2020EA001262

Iron Speciation in $PM_{2.5}$ From Urban, Agriculture, and Mixed Environments in Colorado, USA

Joseph R. Salazar[1], David J. Pfotenhauer[2], Frank Leresche[3], Fernando L. Rosario-Ortiz[3], Michael P. Hannigan[2], Sirine C. Fakra[4], and Brian J. Majestic[1]

[1]Department of Chemistry and Biochemistry, University of Denver, Denver, CO, USA, [2]Department of Mechanical Engineering, University of Colorado Boulder, Boulder, CO, USA, [3]Department of Civil, Environmental, and Architectural Engineering, Environmental Engineering Program, University of Colorado Boulder, Boulder, CO, USA, [4]Advanced Light Source, Lawrence Berkeley National Laboratory, Berkeley, CA, USA

Key Points:
- Large prevalence of the Si-Fe complexes suggests a large contribution from natural, crustal sources
- No observed seasonal change in iron oxidation state
- No observed relationship between iron oxidation state and water-soluble iron

Correspondence to:
B. J. Majestic,
brian.majestic@du.edu

Citation:
Salazar, J. R., Pfotenhauer, D. J., Leresche, F., Rosario-Ortiz, F. L., Hannigan, M. P., Fakra, S. C., & Majestic, B. J. (2020). Iron speciation in $PM_{2.5}$ from urban, agriculture, and mixed environments in Colorado, USA. *Earth and Space Science*, *7*, e2020EA001262. https://doi.org/10.1029/2020EA001262

Received 26 JUN 2020
Accepted 31 AUG 2020
Accepted article online 14 SEP 2020

Abstract Atmospheric iron solubility varies depending on whether the particles are collected in rural or urban areas, with urban areas showing increased iron solubility. In this study, we investigate if the iron species present in different environments affects its ultimate solubility. Field data are presented from the Platte River Air Pollution and Photochemistry Experiment (PRAPPE), aimed at understanding the interactions between organic carbon and trace elements in atmospheric particulate matter (PM). 24-hr $PM_{2.5}$ samples were collected during the summer and winter (2016–2017), at three different sites on the Eastern Colorado plains: an urban, agricultural, and a mixed site. Downtown Denver had an average total and water-soluble iron air concentration of 181.2 and 7.7 ng m^{-3}, respectively. Platteville, the mixed site, had an average of total iron of 76.1 ng m^{-3}, with average water-soluble iron concentration of 9.1 ng m^{-3}. Jackson State Park (rural/agricultural) had the lowest total iron average of 31.5 ng m^{-3} and the lowest water-soluble iron average, 1.3 ng m^{-3}. The iron oxidation state and chemical speciation of 97 samples across all sites and seasons was probed by X-ray absorption near edge structure (XANES) spectroscopy. The most common iron phases observed were almandine ($Fe_3Al_2Si_3O_{12}$) (Denver 21%, Platteville 16%, Jackson 24%), magnetite (Fe_3O_4) (Denver 9%, Platteville 4%, Jackson 5%) and Fe (III)dextran (Denver 5%, Platteville 13%, Jackson 5%), a surrogate for Fe-organic complexes. Additionally, native iron [Fe(0)] was found in significant amounts at all sites. No correlation was observed between iron solubility and iron oxidation state or chemical speciation.

1. Introduction

The presence of iron in the ecosystem has major implications on various geochemical cycles (carbon and sulfur), redox environments, and nutrient availability (Le & Ricard, 1999; Mahowald et al., 2005; Wang & Cappellen, 1996). Iron serves as a necessary nutrient for primary producers, such as algae, and acts as a limiting nutrient in roughly half of the world's oceans (Moore et al., 2013). In both biological and environmental media, the water-soluble iron fraction has been demonstrated to result in the creation of reactive oxygen species (ROS) (Faiola et al., 2011; Hamad et al., 2016; Park et al., 2006), likely generated through Fenton chemistry (Faiola et al., 2011; Kuang et al., 2017; Park et al., 2006). In biological systems, following the inhalation of $PM_{2.5}$ (Brauer et al., 2001), the production of ROS results in oxidative stress to the respiratory system and is suspected to be related to pulmonary inflammation, DNA damage, and the oxidation of proteins and lipids (Landreman et al., 2008; Park et al., 2006; Verma et al., 2014). Given iron's importance from both a health and ecological standpoint, and that these processes are dependent on the availability of iron, the primary driver of this study is to better understand what controls atmospheric iron's solubility.

Iron is the most abundant transition element in the atmosphere and results from windblown dust and urban air pollution (Jickells et al., 2005; Mahowald et al., 2009). Typically, water-soluble iron from crustal sources is less than 1% of the total iron (Paris et al., 2010). This greatly differs from anthropogenic sources where water-soluble iron can range from 5–50% of total iron (Majestic et al., 2007; Petroselli et al., 2018; Salazar et al., 2020; Sedwick et al., 2007; Sholkovitz et al., 2012). The majority of anthropogenic water-soluble iron is estimated to result from combustion sources (Luo et al., 2008). The resulting iron water-solubility is hypothesized to result from an interaction between organics and iron (III) (Haynes & Majestic, 2020; Paris & Desboeufs, 2013; Salazar et al., 2020).

In addition to giving insight into organic-iron interactions, the iron speciation may be an important predictor of its solubility. Synchrotron-based X-ray absorption near edge structure (XANES) spectroscopy has been used to investigate the Fe oxidation state and chemical speciation (iron's surrounding ligands) in ambient PM. Prior reports making use of XANES have attempted to describe the relationship between water-soluble iron and its chemical speciation (Cartledge et al., 2015; Cartledge & Majestic, 2015; Oakes et al., 2012; Takahashi et al., 2011). Several ambient studies observed that Fe (III) is the principal oxidation state in $PM_{2.5}$, primarily as Fe-Al and Fe-Al-Si complexes, originating from windblown dust and soils (Fittschen et al., 2008; Oakes et al., 2012).

In the present campaign, the primary purpose is to better understand how iron speciation and oxidation state can affect iron water solubility across geographical areas and seasons. To achieve this goal, $PM_{2.5}$ was collected from three sites of multiple types: urban, agricultural, and mixed, and in both the winter and the summer. Samples were collected from each site and 97 Fe K-edge XANES spectra in total (31 from Denver [urban], 35 from Platteville [mixed], and 31 Jackson [agricultural]) were analyzed along with total and water-soluble iron. The results were examined to understand if any patterns in season and source influence iron speciation, water-solubility, and oxidation state.

2. Materials and Methods

2.1. Materials Preparation

All vessel cleaning and analytical preparation was performed under a laminar flow hood with incoming air passing through a high-efficiency particulate air (HEPA) filter (NuAire, Plymouth, MN). All water used was purified to 18.2 MΩ-cm (Milli-Q Thermo-Fisher Nanopore). An acid cleaning process was used to prepare the following: 15- and 50-ml plastic centrifuge vials, Petri dishes (Fisher), Teflon forceps (Fisher), syringes (Fisher), and 47 mm Teflon filters. For the plastic centrifuge vials, Petri dishes, Teflon forceps, syringe, and syringe cases this involved 24-hr soaks in a 10% reagent grade nitric acid bath, followed by 10% reagent grade hydrochloric bath, then a 3% trace metal grade nitric acid (Fisher) resting bath with 18.2 MΩ-cm water rinses before, after, and between each step. Syringe filters (0.45-micron) (Whatman, Marlborough, MA) were prepared with 10% trace-metal grade hydrochloric acid, MQ water, and 5% nitric acid rinse. All materials were handled with powder-free nitrile gloves (Fisher), double-bagged.

2.2. Sample Collection

$PM_{2.5}$ was collected at three sites in Colorado's eastern plains: (1) the Colorado Air Monitoring Program (CAMP) site in downtown Denver, an urban setting, (2) Jackson Lake State Park, a rural and agricultural setting, and (3) Platteville Elementary School in Platteville, CO, a mixed agricultural and urban setting that is geographically situated between the other sites (Figure 1).

Air was passed through a cyclone (URG 2000−30 ENB) at 92 L min^{-1}, resulting in a $PM_{2.5}$ size cut. Each site had two sampling lines. One line collected $PM_{2.5}$ on a water cleaned Teflon filter for ion quantification and water-soluble organic experiments. The other sampling line was further split into two lines: one of the lines was collected onto a prebaked quartz filter, and the other line was collected onto an acid-cleaned Teflon filter. The acid-cleaned Teflon filter was used for overall mass determination and trace metal measurements. The total flow was measured for each filter by a flow totalizer (Honeywell BK-G4 Meter).

One campaign was conducted in winter 2016–2017 and one in summer 2017. Samples were collected in 24-hr intervals (midnight to midnight), automated using a 7-day timer (INTERMATIC Electromechanical Timer, 7-Day, SPDT, 21A) every other day in December 2016, February 2017, and August 2017. Exposed Teflon filters were stored in Petri dishes sealed with Teflon tape, double-bagged, and stored in a freezer (−20°C) until analysis.

2.3. Water-Soluble Element Preparation

Water-soluble iron was extracted from the Teflon filters for 12 hr on a shaker table in 15 ml of 18.2 MΩ-cm water. The water extract was filtered with 0.45 μm pore size polyethersulfone (PES) syringe filters. This filtered water-soluble extract was acidified to 5% trace-metal grade nitric acid and 2.5% trace-metal grade hydrochloric acid and analyzed by inductively coupled plasma mass spectrometry (ICP-MS, Agilent 7,700).

Figure 1. Map of the three sampling site CAMP, Jackson, and Platteville (Source: Google Maps).

2.4. Elemental Analysis

The polymethylpentene ring was removed from the Teflon filters and about 4% (measured exactly) of the filter was removed and used for Fe XANES spectroscopy. The remaining (~96%) Teflon filter for each sample was placed into a microwave digestion vessel. In each digestion vessel, 750 μL of concentrated trace metal grade nitric acid, 250 μL of concentrated trace metal grade hydrochloric acid, 100 μL of concentrated trace metal grade hydrofluoric acid, and 100 μL of 30% hydrogen peroxide were added. The filters with the collected $PM_{2.5}$ were digested (Ethos EZ, Milestone Inc.) according to the following temperature program: 15-min ramp to 200°C, then held at 200°C for 25 min, and a 60-min cooling period (Cartledge & Majestic, 2015). Finally, the solution was removed and diluted to 15 mL with MQ water and analyzed via ICP-MS.

Blank filters and standard reference materials (SRMs) were digested alongside the collected $PM_{2.5}$ using the same digestion process described above. Two SRMs were used to address the recoveries of Fe in the digestion process: urban particulate matter (1648a, NIST) and San Joaquin Soil (2709a, NIST). The recoveries of the SRMs were between 80% and 120%. Indium (~1 ppb) was used as an internal standard and a He collision cell was used to remove polyatomic interferences.

2.5. XANES Spectroscopy

Fe K-edge X-ray absorption near-edge structure (XANES) and X-ray fluorescence (XRF) mapping data for 39 samples were collected at the Advanced Light Source Microprobe beamline (10.3.2), at Lawrence Berkeley National Laboratory, Berkeley, CA (Marcus et al., 2004). A broad XRF map of each sample was acquired at 10 keV with 20 μm by 20 μm pixel size and 80 ms dwell time per pixel to locate the concentrated iron spots on the filter. Where iron was concentrated, a fine map was collected with 8 μm by 8 μm pixel size and 80 ms dwell time per pixel. From this map, 2–3 iron spots per filter were chosen for Fe K-edge extended XANES analysis (totaling 97 spectra). All data were recorded using a seven-element solid state Ge detector (Canberra, ON) in fluorescence mode by continuously scanning the Si (111) monochromator (Quick XAS mode) in the range of 7,010–7,415 eV. The spectra were then deadtime corrected, deglitched, calibrated, pre-edge background subtracted and post-edge normalized using a suite of LabVIEW custom programs (Marcus et al., 2008) available at the beamline. Spectra were calibrated using an iron foil with first

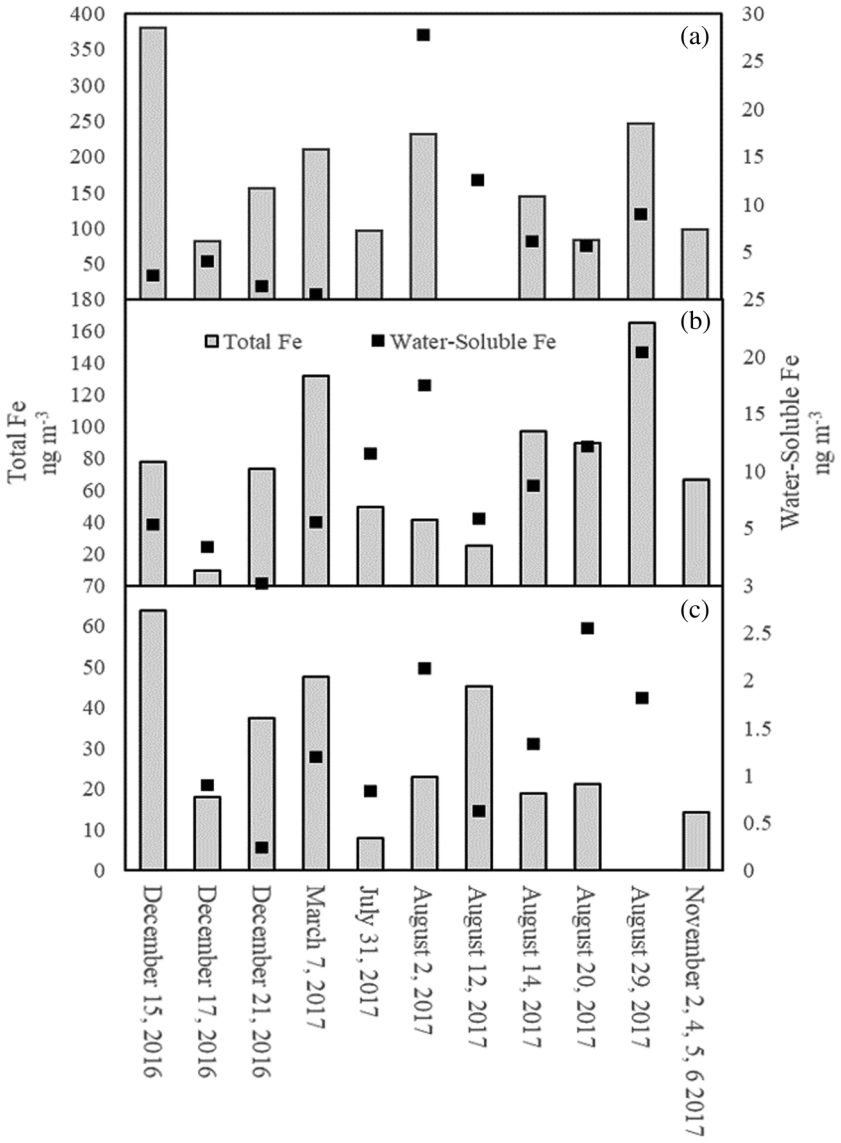

Figure 2. Total and water-soluble iron including sampling days from winter and summer. All samples were collected for 24-hr, except for November 2 and 4–6, 2017, which was a 4-day sample. November 2 and 4–6, 2017, was not tested for water-soluble iron. (a) Denver. 31 July 2017 water-soluble iron was removed due to operational error in collection. (b) Platteville. (c) Jackson site.

derivative maximum set at 7,110.75 eV (Kraft et al., 1996). Least squares linear combination fitting (LCF) was performed in the range 7,090 to 7,365 eV to identify oxidation states and iron speciation following methods previously described in (Westphal et al., 2009) using a large updated 10.3.2 XAS database of Fe bearing compounds and custom LabVIEW software available at the beamline. Determination of the mineral groups and in some cases mineral identity can be obtained (+/− 10% error estimate). Fe valence scatter plots were generated from Fe XANES data, producing a two-dimensional plot where each datapoint represents a XANES spectrum, following procedures described elsewhere (Marcus et al., 2008). Note that this technique needs to be applied in conjunction with LCF to confirm Fe valence.

3. Results

3.1. Water-Soluble Iron and Total Iron

Total and water-soluble iron from each region (urban, agricultural, and mixed) differed in averages and from day to day, and the results for all sites are presented in Figure 2. Across all seasons, downtown Denver had an

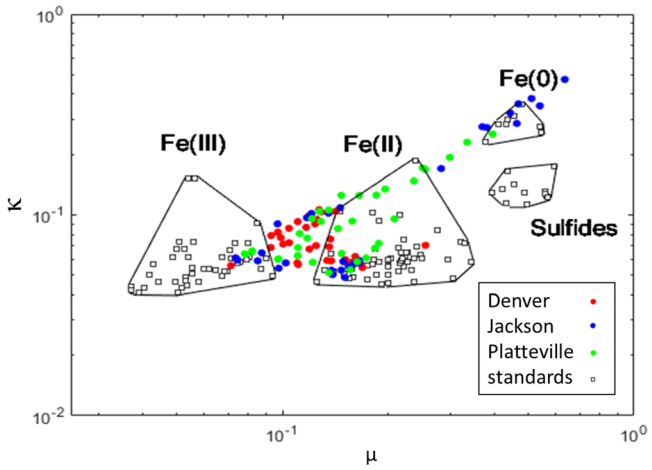

Figure 3. Iron valence scatter plot generated from Fe K-edge XANES data where κ and μ are normalized absorbance values at 7,113 and 7,117.5 eV, respectively. Open black squares represent iron standards of known valence while the red dots are the Denver site (urban), blue dots are Jackson (agricultural), and green dots are Platteville (mixed).

average of total iron of 181.2 ng m^{-3} (range: 80.9–380.5 ng m^{-3}) and an average of water-soluble iron of 7.7 ng m^{-3}, or 4.2% of total iron (range: 0.5–27.8 ng m^{-3}). Platteville had an average of total iron of 76.1 ng m^{-3} (range: 9.6–165.6 ng m^{-3}) and average water-soluble iron of 9.1 ng m^{-3}, or 11.9% of total iron (range: 0.2–20.3 ng m^{-3}). Jackson State Park, the agricultural site, had the lowest total iron average of 31.5 ng m^{-3} (range: 7.9–63.7 ng m^{-3}) and the lowest water-soluble iron average, 1.3 ng m^{-3}, or 4.1% of total iron (range: 0.2–2.5 ng m^{-3}).

The extent of seasonal variations differs for the total and the water-soluble iron (t test, $p < 0.05$). Across all sites, winter had lower water-soluble iron with the average being 2.3 ng m^{-3} (range; 0.17–5.6 ng m^{-3}), while summer average of 8.6 ng m^{-3} (range; 0.6–27.8 ng m^{-3}). For total iron, however, winter was greater than the summer, on average. The winter average was 107.3 ng m^{-3} (range; 9.6–380.5 ng m^{-3}), and the summer average was 86.8 ng m^{-3} (range; 7.9–247.2 ng m^{-3}). Across all sites, iron fractional solubility for the winter was 2.1% and for the summer, it was 9.9%.

3.2. Iron Oxidation States

An initial valence state scatter plot was generated using iron's K edge normalized XANES data to quickly classify particles according to iron oxidation states (Figure 4). The oxidation states observed were Fe(0), Fe (II), Fe (III), and mixed [a mixture of both Fe (II) and Fe (III)]. On a relative basis, the Jackson site observed the most Fe(0) and Fe (II) with less of the mixed and Fe (III). The Platteville site showed a large amount of Fe (II) and mixed iron phases. Denver had most samples fall in the mixed region followed by Fe (III) and then Fe (II).

A mixture of multiple iron mineral groups can be found for the iron that falls into the mixed oxidation state region in the valence plot. Using LCF, the fraction of Fe (II) and Fe (III) that are in the mixed area of the valence plot were obtained, adding more detail to the chemical speciation of iron in this region (Figure 5). Figure 5 shows two example Fe-XANES plots showing the weighted iron standards involved in the LCF of the data. These percentages were obtained for each by summing the percentages for each oxidation state. Fe with mixed oxidation state were labeled as "mixed oxidation state." The average oxidation states for each iron sample per site are as follows: Denver Fe (III) 37%, Denver Fe (II) 39%, Platteville Fe (III) 44%, Platteville Fe (II) 32%, Jackson Fe (III) 27%, and Jackson Fe (II) 34%. Fe(0) was ubiquitous at all three sites, but to varying degrees: Jackson 27%, Platteville 13%, and Denver 3%. Fe (II) and Fe (III) were also compared between winter and summer for all sites. Fe (II) was shown to be 31% of all particles tested in the winter. In the summer, Fe (II) accounted for 39% of the total iron tested. Fe (III) was found to be 39% in the winter of iron and in the summer Fe (III) shown to be 30% of iron.

As Fe (II) is generally more water-soluble than Fe (III), the particle-bound oxidation states were compared to the percent water-soluble iron. Fe (II) and water-soluble iron by day showed no significant relationship

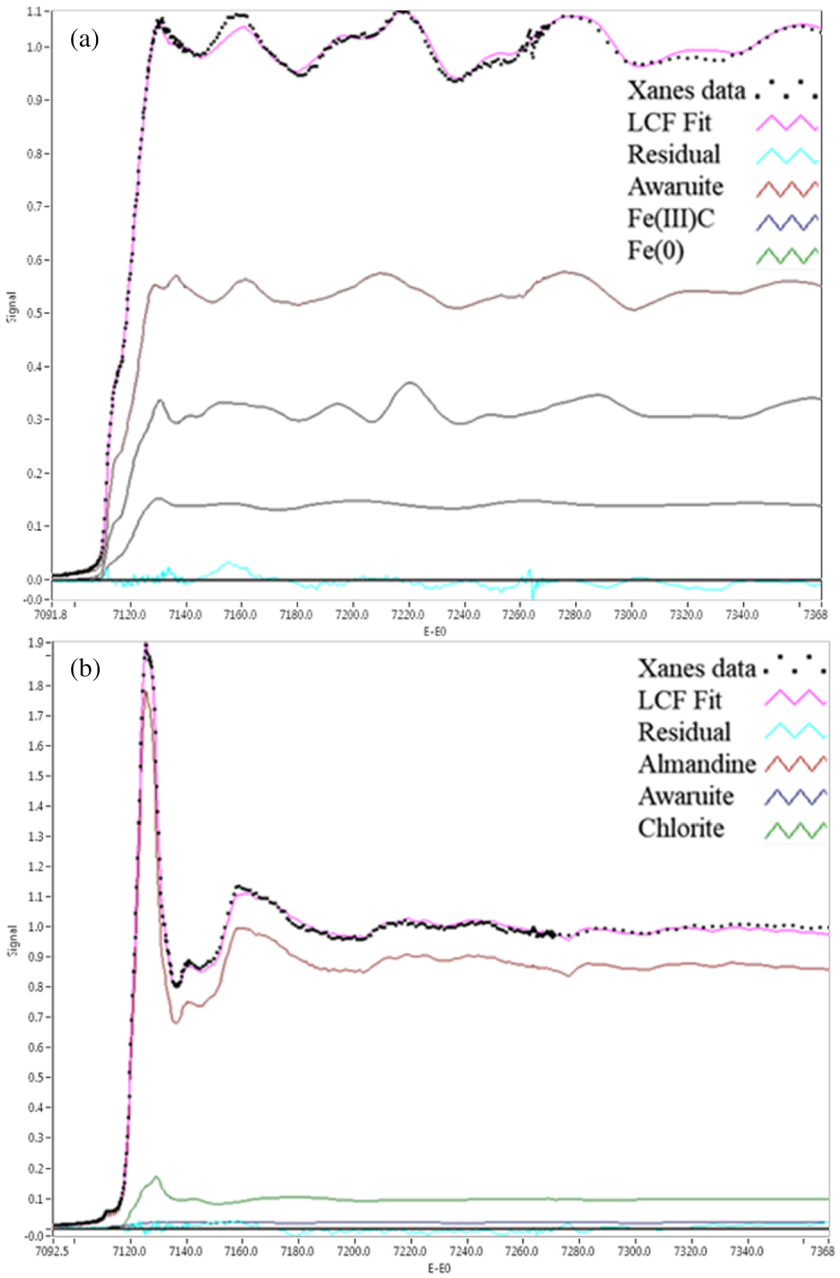

Figure 4. Examples of least squares linear combination fitting (LCF) and respective weighted plots of the components or for the LCF of XANES plots. The components used in the fit are mineral standards measured at the ASL beam line 10.3.2. (a) Sample collected on 17 December 2016 at Jackson Lake State Park LCF is composed of 54.2% awaruite, 14.2% Fe (III), and 31.7 Fe(0). (b) Sample collected on 30 August 2017 at Jackson Lake State Park LCF is composed of 87.2% almandine trace amount of awaruite and chlorite.

($R^2 = 0.03$). Fe (III) was tested against water-soluble iron and no relationship was found between Fe (III) and water-soluble iron ($R^2 = 0.00$). Generally, no relationship between iron solubility and particle-bound oxidation state was observed for any iron species.

3.3. Iron Mineralogy

As no correlation was found between the iron oxidation state and its water-solubility, we probed deeper by investigating how iron speciation (i.e., ligands and immediate chemical environment) may affect the water solubility. From the XANES spectra and the LCF, the percent of iron species were defined for each iron spot,

Table 1
Fraction of Top Eight Iron Species for Each Site

LCF of iron mineral groups	Denver	Platteville	Jackson
Almandine	21%	16%	24%
Magnetite	9%	4%	5%
Fe (III)dextran	5%	13%	5%
Feroxyhite	5%	3%	0%
Coalingite	5%	4%	4%
Fe biogenic oxide	5%	5%	0%
Hematite	3%	3%	5%
Kaolinite	2%	6%	6%

then averaged together to look at the most common iron species for each site (Table 1). The most common iron species for all three sites was the mineral almandine ($Fe_3Al_2Si_3O_{12}$), which is an iron-aluminum-silicate complex. Almandine accounted for 21% of iron particles in Denver, 16% of iron particles in Platteville, and 24% of iron particles in Jackson. The second most common iron species was magnetite (Fe_3O_4) with 9% in Denver, 4% in Platteville, and 5% in Jackson. The third most common iron species was Fe (III)dextran, a surrogate for an iron-organic complex, which accounted for 5% of iron in Denver and Jackson and 13% of iron in Platteville.

4. Discussion

4.1. Total and Water-Soluble Iron

The Colorado Coarse Rural-Urban Sources and Health (CCRUSH) study found that, in residential neighborhoods in Denver, total iron in $PM_{2.5}$ was 89 ng m^{-3} at Alsup Elementary and 56 ng m^{-3} Edison Elementary (Clements et al., 2014). These locations were in different parts of Denver at distances less than 11 km from the CAMP sampling site. These concentrations were less than the average 181.2 ng m^{-3} measured in this study. In 2014, another study done in the same Denver location as the current study showed an average iron in $PM_{2.5}$ of 190 ng m^{-3} (Clements et al., 2014). This result illustrates the difference in concentrations in downtown versus residential neighborhoods within a major metropolitan area. Water-soluble iron was also measured in Denver in 2012 January to February averaging 29 ng m^{-3} which is more than the 7.7 ng m^{-3} measured in this study. However, those samples were extracted in a 0.5 mM acetate buffer (pH = 4.25) compared to the pure 18.2 MΩ-cm water used here, and the acetate buffer is known to give a higher iron solubility compared to pure water (Cartledge & Majestic, 2015; Majestic et al., 2006).

Iron water-solubility and oxidation state were examined for summer and winter. There was no change for iron oxidation state in winter and summer. Iron water-solubility was 3.8 times higher in the summer (8.6 ng m^{-3}) than in the winter (2.3 ng m^{-3}). Water-soluble iron was not correlated to either particle-bound Fe (II) or Fe (III). This evidence indicates that iron oxidation state is not a factor in iron solubility. In the summer, we observed increased iron solubility, with a decreased total iron load, relative to winter. This scenario is consistent with the iron being derived from a pyrogenic source (Sholkovitz et al., 2012), probably from the record-breaking (at the time) wild fires prevalent across the Western United States, which historically impact the air quality at this study's test sites (Creamean et al., 2016).

4.2. Mineralogy

A surprisingly high fraction of the Fe found in Jackson (27%) and Platteville (13%) is in the native Fe(0) oxidation state. In solution, Fe(0) produces the most ROS compared with Fe (II) and Fe (III) (Phenrat et al., 2009). To our knowledge, this is the first study to measure native iron in the atmosphere in any significant amount.

Fe (II) aluminosilicates were found to be the most common form of iron at all three sites. Because of the association with aluminum and silicate, this shows that at least 20% of iron found in $PM_{2.5}$ in eastern Colorado is from crustal sources. Fe (II) aluminum silicate complexes have been previously found in other geographical areas (Oakes et al., 2012; Petroselli et al., 2018). Petroselli et al. collected a $PM_{2.5}$ sample near a steel plant in Terni, Italy and measured Fe (III) as the predominate species in this sample. Oakes et al. collected four samples in both rural and urban sites and, similar to the results presented here, found a large amount of Fe-aluminosilicates in all sites and did not show a variation in iron speciation from the two sites, an effect attributed to low sample size. Here, we had a larger sample size and observed no seasonal variation with respect to Fe- aluminosilicates, which helps to confirm the results from Oakes et al.

Magnetite, a mixed Fe (II,III) oxide has been found to originate from diesel vehicles and is also present in crustal sources (Abdul-Razzaq & Gautam, 2001; Oakes et al., 2012; Petroselli et al., 2018). Here we identified magnetite in 9% of iron tested in Denver, 5% in Platteville, and 4% in Jackson (Table 1). The increase of magnetite in Denver suggests that it can originate from vehicular activity in Denver. There is less evidence for

magnetite being related diesel vehicles in Platteville and Jackson resulting from showing lower percentages of magnetite.

Fe (III)dextran is an iron-sugar complex. While likely not directly found in the atmosphere, Fe (III)dextran is used as a surrogate for iron complexed to oxidized organic species. Water-soluble Fe has been hypothesized to primarily result from biomass burning, whose emissions contain sugars like levoglucosan, mannosan, and galactosan (Scaramboni et al., 2015). Concentration of sugars from biomass burning can range from 6 ng m^{-3} to 12.5 μg m^{-3} (Scaramboni et al., 2015; Theodosi et al., 2018), and they are highly water-soluble (Barbaro et al., 2019; Simoneit et al., 2004). Water-solubilization of iron by theses sugar complexes in biomass burning fumes could be a large contributor to total water-soluble iron. However, since these organic biomass sugar compounds were not measured in this study, this could not be directly tested here.

5. Conclusion

Atmospheric iron was probed from three different environments in the eastern plains of Colorado. The most common mineral found was almandine, which accounted for 20% of total iron tested. The large prevalence of the Si-Fe complexes suggests a large contribution from natural, crustal sources, even within urban areas. Fe (III)dextran, an organic iron complex and magnetite were also abundant. Iron oxidation states were compared seasonally, where no change in oxidation state was observed; however, an increase in iron water-solubility was present in the summer. Finally, water-soluble iron was compared to Fe (II) and Fe (III), and results indicated there is no relationship between iron oxidation state and water-soluble iron.

There was no observed relationship between atmospheric iron solubility and the chemical speciation of iron at any of the sites. This result suggests that overall atmospheric iron is dependent on other factors aside from its oxidation state and chemical speciation. Previous studies have shown that the pH of the extract solution is an important parameter in addressing iron solubility (Stumm & Morgan, 1996). Therefore, nonferrous acid-base active species may be important contributors to the solubility in aqueous extracts. Additionally, iron may be solubilized by interactions with organic compounds that are present in the aerosol and, thus, the extract solution. Recent studies have shown that aerosols rich in specific combustion-derived organic species lead to increased aqueous iron solubility (Ito et al., 2019; Salazar et al., 2020). To fully understand atmospheric iron solubility, it is becoming clearer that researchers must look at contributing species, such as organics and pH-active compounds, and not solely at the iron.

Data Availability Statement

Data archiving is provided at the Digital Commons @ DU (https://digitalcommons.du.edu), with this data set residing at this site (https://digitalcommons.du.edu/chemistrydatasets/1/). These data sets are publicly available and contain the raw ICPMS and XANES data, along with the least squares fitting results.

Acknowledgments
The authors thank the Colorado Department of Public Health and Environment for the use of the air monitoring facility. This study was funded by National Science Foundation Grant 1549166. This research used resources of the Advanced Light Source, which is a DOE Office of Science User Facility under Contract DE-AC02-05CH11231.

References

Abdul-Razzaq, W., & Gautam, M. (2001). Discovery of magnetite in the exhausted material from a diesel engine. *Applied Physics Letters*, *78*(14), 2018–2019. https://doi.org/10.1063/1.1358357

Barbaro, E., Feltracco, M., Cesari, D., Padoan, S., Zangrando, R., Contini, D., et al. (2019). Characterization ofthewater soluble fraction in ultrafine, fine, and coarse atmospheric aerosol. *Science of the Total Environment*, *658*, 1423–1439. https://doi.org/10.1016/j.scitotenv.2018.12.298

Brauer, M., Avila-Casado, C., Fortoul, T. I., Vedal, S., Stevens, B., & Churg, A. (2001). Air pollution and retained particles in the lung. *Environmental Health Perspectives*, *109*(10), 1039–1043. https://doi.org/10.1289/ehp.011091039

Cartledge, B. T., & Majestic, B. J. (2015). Metal concentrations and soluble iron speciation in fine particulate matter from light rail activity in the Denver-metropolitan area. *Atmospheric Pollution Research*, *6*(3), 495–502. https://doi.org/10.5094/APR.2015.055

Cartledge, B. T., Marcotte, A. R., Herckes, P., Anbar, A. D., & Majestic, B. J. (2015). The impact of particle size, relative humidity, and Sulfur dioxide on Iron solubility in simulated atmospheric marine aerosols. *Environmental Science and Technology*, *49*(12), 7179–7187. https://doi.org/10.1021/acs.est.5b02452

Clements, N., Eav, J., Xie, M., Hannigan, M. P., Miller, S. L., Navidi, W., et al. (2014). Concentrations and source insights for trace elements in fine and coarse particulate matter. *Atmospheric Environment*, *89*, 373–381. https://doi.org/10.1016/j.atmosenv.2014.01.011

Creamean, J. M., Neiman, P. J., Coleman, T., Senff, C. J., Kirgis, G., Alvarez, R. J., & Yamamoto, A. (2016). Colorado air quality impacted by long-range-transported aerosol: A set of case studies during the 2015 Pacific northwest fires. *Atmospheric Chemistry and Physics*, *16*(18), 12,329–12,345. https://doi.org/10.5194/acp-16-12329-2016

Faiola, C., Johansen, A. M., Rybka, S., Nieber, A., Thomas, C., Bryner, S., et al. (2011). Ultrafine particulate ferrous iron and anthracene associations with mitochondrial dysfunction. *Aerosol Science and Technology*, *45*(9), 1109–1122. https://doi.org/10.1080/02786826.2011.581255

Fittschen, U. E. A., Meirer, F., Streli, C., Wobrauschek, P., Thiele, J., Falkenberg, G., & Pepponi, G. (2008). Characterization of atmospheric aerosols using synchroton radiation total reflection X-ray fluorescence and Fe K-edge total reflection X-ray fluorescence-X-ray absorption near-edge structure. *Spectrochimica Acta Part B: Atomic Spectroscopy*, *63*(12), 1489–1495. https://doi.org/10.1016/j.sab.2008.10.016

Hamad, S. H., Schauer, J. J., Antkiewicz, D. S., Shafer, M. M., & Kadhim, A. K. H. (2016). ROS production and gene expression in alveolar macrophages exposed to PM2.5 from Baghdad, Iraq: Seasonal trends and impact of chemical composition. *Science of the Total Environment*, *543*, 739–745. https://doi.org/10.1016/j.scitotenv.2015.11.065

Haynes, J., & Majestic, B. (2020). Role of polycyclic aromatic hydrocarbons on the photo-catalyzed solubilization of simulated soil-bound atmospheric iron. *Atmospheric Pollution Research*, *11*(3), 583–589. https://doi.org/10.1016/j.apr.2019.12.007

Ito, A., Myriokefalitakis, S., Kanakidou, M., Mahowald, N. M., Scanza, R. A., Hamilton, D. S., et al. (2019). Pyrogenic iron: The missing link to high iron solubility in aerosols. *Science Advances*, *5*(5), eaau7671. https://doi.org/10.1126/sciadv.aau7671

Jickells, Z. S. A., Andersen, K. K., Baker, A. R., Bergametti, G., Brooks, N., Cao, J. J., et al. (2005). Global iron concentrations between desert dust, ocean biogeochemistry, and climate. *Science*, *308*(5718), 67–71. https://doi.org/10.1126/science.1105959

Kraft, S., Stümpel, J., Becker, P., & Kuetgens, U. (1996). High resolution x-ray absorption spectroscopy with absolute energy calibration for the determination of absorption edge energies. *Review of Scientific Instruments*, *67*(3), 681–687. https://doi.org/10.1063/1.1146657

Kuang, X. M., Scott, J. A., da Rocha, G. O., Betha, R., Price, D. J., Russell, L. M., et al. (2017). Hydroxyl radical formation and soluble trace metal content in particulate matter from renewable diesel and ultra low sulfur diesel in at-sea operations of a research vessel. *Aerosol Science and Technology*, *51*(2), 147–158. https://doi.org/10.1080/02786826.2016.1271938

Landreman, A. P., Shafer, M. M., Hemming, J. C., Hannigan, M. P., & Schauer, J. J. (2008). A macrophage-based method for the assessment of the reactive oxygen species (ROS) activity of atmospheric particulate matter (PM) and application to routine (Daily-24 h) aerosol monitoring studies. *Aerosol Science and Technology*, *42*(11), 946–957. https://doi.org/10.1080/02786820802363819

Le, C., & Ricard, Y. (1999). Long-Term Fluxes and Budget of Ferric Iron: Implication for the Redox States of the Earth's Mantle and Atmosphere. *Earth and Planetary Science Letters*, *165*, 197–211. https://doi.org/10.1016/s0012-821x(98)00267-2

Luo, C., Mahowald, N., Bond, T., Chuang, P. Y., Artaxo, P., Siefert, R., et al. (2008). Combustion iron distribution and deposition. *Global Biogeochemical Cycles*, *22*, GB1012. https://doi.org/10.1029/2007GB002964

Mahowald, N., Baker, A. R., Bergametti, G., Brooks, N., Duce, R. A., Jickells, T. D., et al. (2005). Atmospheric global dust cycle and iron inputs to the ocean. *Global Biogeochemical Cycles*, *19*, GB4025. https://doi.org/10.1029/2004GB002402

Mahowald, N. M., Engelstaedter, S., Luo, C., Sealy, A., Artaxo, P., Benitez-Nelson, C., et al. (2009). Atmospheric iron deposition: Global distribution, variability, and human perturbations. *Annual Review of Marine Science*, *1*(1), 245–278. https://doi.org/10.1146/annurev.marine.010908.163727

Majestic, B. J., Schauer, J. J., & Shafer, M. M. (2007). Application of synchrotron radiation for measurement of iron red-ox speciation in atmospherically processed aerosols. *Atmospheric Chemistry and Physics*, *7*(Iii), 2475–2487. https://doi.org/10.5194/acpd-7-1357-2007

Majestic, B. J., Schauer, J. J., Shafer, M. M., Turner, J. R., Fine, P. M., Singh, M., & Sioutas, C. (2006). Development of a wet-chemical method for the speciation of iron in atmospheric aerosols. *Environmental Science and Technology*, *40*(7), 2346–2351. https://doi.org/10.1021/es052023p

Marcus, M. A., Macdowell, A. A., Celestre, R., Manceau, A., Miller, T., Padmore, H. A., & Sublett, R. E. (2004). Beamline 10.3.2 at ALS: A hard X-ray microprobe for environmental and materials sciences. *Journal of Synchrotron Radiation*, *11*(3), 239–247. https://doi.org/10.1107/S0909049504005837

Marcus, M. A., Westphal, A. J., & Fakra, S. C. (2008). Classification of Fe-bearing species from K-edge XANES data using two-parameter correlation plots. *Journal of Synchrotron Radiation*, *15*(5), 463–468. https://doi.org/10.1107/S0909049508018293

Moore, J. K., Lindsay, K., Doney, S. C., Long, M. C., & Misumi, K. (2013). Marine Ecosystem Dynamics and Biogeochemical Cycling in the Community Earth System Model [CESM1(BGC)]: Comparison of the 1990s with the 2090s under the RCP4.5 and RCP8.5 Scenarios. *Journal of Climate*, *26*(23), 9291–9312. https://doi.org/10.1175/JCLI-D-12-00566.1

Oakes, M., Weber, R. J., Lai, B., Russell, A., & Ingall, E. D. (2012). Characterization of iron speciation in urban and rural single particles using XANES spectroscopy and micro X-ray fluorescence measurements: Investigating the relationship between speciation and fractional iron solubility. *Atmospheric Chemistry and Physics*, *12*(2), 745–756. https://doi.org/10.5194/acp-12-745-2012

Paris, R., & Desboeufs, K. V. (2013). Effect of atmospheric organic complexation on iron-bearing dust solubility. *Atmospheric Chemistry and Physics*, *13*(9), 4895–4905. https://doi.org/10.5194/acp-13-4895-2013

Paris, R., Desboeufs, K. V., Formenti, P., Nava, S., & Chou, C. (2010). Chemical characterisation of iron in dust and biomass burning aerosols during AMMA-SOP0/DABEX: Implication for iron solubility. *Atmospheric Chemistry and Physics*, *10*(9), 4273–4282. https://doi.org/10.5194/acp-10-4273-2010

Park, S., Nam, H., Chung, N., Park, J.-D., & Lim, Y. (2006). The role of iron in reactive oxygen species generation from diesel exhaust particles. *Toxicology in Vitro*, *20*(6), 851–857. https://doi.org/10.1016/j.tiv.2005.12.004

Petroselli, C., Moroni, B., Crocchianti, S., Selvaggi, R., Vivani, R., Soggia, F., et al. (2018). Iron speciation of natural and anthropogenic dust by spectroscopic and chemical methods. *Atmosphere*, *10*(1), 8. https://doi.org/10.3390/atmos10010008

Phenrat, T., Long, T., Gregory, L., & Veronesi, B. (2009). Partial oxidation ("aging") and surface modification decrease the toxicity of Nanosized Zerovalent Iron. *Environmental Science & Technology*, *42*, 195–200. https://doi.org/10.1021/es801955n

Salazar, J. R., Cartledge, B. T., Haynes, J. P., York-Marini, R., Robinson, A. L., Drozd, G. T., et al. (2020). Water-soluble iron emitted from vehicle exhaust is linked to primary speciated organic compounds. *Atmospheric Chemistry and Physics*, *20*, 1849–1860. https://doi.org/10.5194/acp-20-1849-2020

Scaramboni, C., Urban, R. C., Lima-souza, M., Nogueira, R. F. P., Cardoso, A. A., Allen, A. G., & Campos, M. L. A. M. (2015). Total sugars in atmospheric aerosols: An alternative tracer for biomass burning. *Atmospheric Environment*, *100*, 185–192. https://doi.org/10.1016/j.atmosenv.2014.11.003

Sedwick, P. N., Sholkovitz, E. R., & Church, T. M. (2007). Impact of anthropogenic combustion emissions on the fractional solubility of aerosol iron: Evidence from the Sargasso Sea. *Geochemistry, Geophysics, Geosystems*, *8*, Q10Q06. https://doi.org/10.1029/2007GC001586

Sholkovitz, E. R., Sedwick, P. N., Church, T. M., Baker, A. R., & Powell, C. F. (2012). Fractional solubility of aerosol iron: Synthesis of a global-scale data set. *Geochimica et Cosmochimica Acta*, *89*, 173–189. https://doi.org/10.1016/j.gca.2012.04.022

Simoneit, B. R. T., Kobayashi, M., Kawamura, K., Rushdi, A. I., Rogge, W. F., & Didyk, B. M. (2004). Sugars S dominant water-soluble organic compounds in soils and characterization as tracers in atmospheric particulate matter. *Environmental Science & Technology*, *38*(22), 5939–5949. https://doi.org/10.1021/es0403099

Stumm, W., & Morgan, J. J. (1996). *Aquatic chemistry: chemical equilibria and rates in natural waters* (3rd ed.). New York: Wiley.

Takahashi, Y., Higashi, M., Furukawa, T., & Mitsunobu, S. (2011). Change of iron species and iron solubility in Asian dust during the long-range transport from western China to Japan. *Atmospheric Chemistry and Physics*, *11*, 11,237–11,252.

Theodosi, C., Panagiotopoulos, C., Nouara, A., Zarmpas, P., Nicolaou, P., & Violaki, K. (2018). Progress in oceanography sugars in atmospheric aerosols over the Eastern Mediterranean. *Progress in Oceanography*, *163*(July 2016), 70–81. https://doi.org/10.1016/j.pocean.2017.09.001

Verma, V., Fang, T., Guo, H., King, L., Bates, J. T., Peltier, R. E., et al. (2014). Reactive oxygen species associated with water-soluble PM2.5 in the southeastern United States: Spatiotemporal trends and source apportionment. *Atmospheric Chemistry and Physics*, *14*(23), 12,915–12,930. https://doi.org/10.5194/acp-14-12915-2014

Wang, Y., & Cappellen, P. V. A. N. (1996). A multicomponent reactive transport model of early diagenesis: Application to redox cycling in coastal marine sediments. *Geochimica et Cosmochimica Acta*, *60*(16), 2993–3014. https://doi.org/10.1016/0016-7037(96)00140-8

Westphal, A. J., Fakra, S. C., Gainsforth, Z., Marcus, M. A., Ogliore, R. C., & Butterworth, A. L. (2009). Mixing fraction of inner solar system material in comet 81P/Wild2. *Astrophysical Journal*, *694*(1), 18–28.